Dose rates as a function of distance from an extended and shielded source exhibit a functional behavior different from standard, less complex source geometries.

Investigation of Dose Rates Exterior to an Above-Ground Waste Storage Facility Using Radiation Transport Models

Jenelle Elicia Mann, Norbert Zoeger, Roman Koppitsch, and Alexander Brandl[1]

Abstract: *The dose rate profile at different heights above the ground and as a function of distance from the north, west, and south walls of an above-ground waste storage facility was analyzed using the Monte Carlo n-Particle Transport eXtended (MCNPX) radiation transport code. The waste storage facility houses 9,996 waste barrels of conditioned waste. The facility has concrete shielding added to the building walls on the north, west, and east sides, with no such additional shielding towards the roof or the south side wall; instead, the distance from the first row of barrels to the wall is extended to allow for maneuverability of a crane on the south side. The dose rate is computed as a function of distance using MCNPX and assuming a homogeneous ^{60}Co distribution in each waste barrel. Different dose regions are identified and analyzed based on graphical features and best-fit functions. The dose rates were expected to be largest at the wall of the facility and subsequently decrease continuously with distance from the repository; however, our analysis indicates a peak in dose rate observed for all heights on the north and west sides of the facility. This peak is likely due to scattering in the shielding material and atmosphere, and possibly could be ascribed to skyshine. The difference between the dose rate at 1 m outside the wall and the peak dose rate is significant, and indicates that the dose rate measured close to the wall may not always be conservative for extended sources, such as an above-ground waste storage facility. Health Phys. 115(4):539–544; 2018*

Key words: *operational topics; dosimetry, external; modeling, dose assessment; waste storage*

INTRODUCTION

During the handling, storage, and disposal of radioactive materials, it is crucial to know the approximate dose rates due to these sources of ionizing radiation to keep doses to workers and the public as low as reasonably achievable (ALARA). The dose rate surrounding radioactive sources depends on the geometry of the source, source emission type, and source energy. For simple sources, the dose rate as a function of position can be derived analytically. However, for most source geometries, Monte Carlo or numerical analysis is necessary to calculate the dose rate as a function of position with respect to the source. In this paper, the photon dose rate profile surrounding an above-ground waste storage facility is investigated using the Monte Carlo N-Particle Transport eXtended (MCNPX) code (MCNP Team 2008).

The photon dose rate at a given detector due to a photon emitting radionuclide depends on the fluence rate, the photon energy, and the photon energy absorption characteristics of the materials between the source and the detector, where the fluence rate at the detector location depends on the solid angle subtended by the detector with respect to the source and any scattering material between the source and the detector. The subtended solid angle previously was derived analytically for on and off center line sources, planar sources (Johnson and Birky 2012), circular disks (Gardner and Carnesale 1969; Rizk et al. 1986), right circular cylinders (Verghese et al. 1972), circular apertures (Jaffey 1954), and rectangular slits (Gotoh and Yagi 1971). Solid angle calculations using Monte Carlo techniques have been described in general (Carchon et al. 1975) and have been applied for disk sources (Williams 1966; Bonnet et al. 1967) and right circular cylinders (Green et al. 1974; Carchon et al. 1975; Wielopolaki 1977).

In the case of a point or a planar source with a point detector, the fluence rate (subtended solid angle) decreases as r^{-2} and r^{-1} for a distance r from the source, respectively.

[1]*Colorado State University, Fort Collins, CO.*

The authors declare no conflicts of interest.

Jenelle Mann received her PhD in radiological health sciences specializing in health physics from Colorado State University in 2016. Ms. Mann has research experience in simulation of spectral anomaly algorithm performance for radiological emergency response equipment, modeling occupational exposure situations using Monte Carlo Codes, evaluation of plant uptake and effectiveness of biological remediation substances, and improvement of deterministic dosimetry codes. Her email address is ***Jenelle.e.mann@gmail.com****.*

Dose rates as a function of distance from an extended and shielded source exhibit a functional behavior different from standard, less complex source geometries.
(Manuscript accepted 6 April 2018)

Copyright © 2018 Health Physics Society. Unauthorized reproduction of this article is prohibited.

When the detector location is sufficiently far from the area or volume source, it can be approximated as a point source. However, the distance at which this approximation is valid is not clearly defined. The deviation from the true functional dependence for such an approximation was calculated by for line and disk sources at one, two, and three times the maximum dimensions of the source (Bevelacqua 2004). The deviation is largest at one times the maximum dimension of the source, at 8% for a line source and 12% for a disk source (Bevelacqua 2004). It decreases to 2% and 3% for a line and a disk source, respectively, at twice the maximum dimension, and to 1% at three times the maximum dimension (Bevelacqua 2004). For area and volume sources, a distance of at least twice the largest dimension of the source is recommended for the point source approximation to be valid (Johnson and Birky 2012).

For large sources, such as a waste storage facility, where people work closer to the source than the largest dimension of the source, estimating the source as a point source may not be sufficient. Dose rates have been modeled extensively using Monte Carlo methods for radiation therapy dosimetry and instrument response (Rogers 2006). Monte Carlo simulations have also been analyzed for a wide range of occupational exposure scenarios, including interventional radiology (Koukorava et al. 2011; Siiskonen et al. 2014), cooling circuits of a fusion power plant (Forty 1996), removal of reactor components from a research reactor pool (Kontogeorgakos et al. 2011), and a standard waste barrel arrangement for transport (Zoeger and Brandl 2011).

In this paper, the dose rate profile for an above ground interim waste storage facility is developed. The facility analyzed is based on the Austrian Interim Radiological Waste Storage Facility at the Austrian Institute of Technology at Seibersdorf, operated by Nuclear Engineering Seibersdorf. Dose rates are analyzed using Monte Carlo simulations for distances between 0 and up to 750 m from the facility. The simulated dose rates are fitted using analytic functions.

METHODS AND MATERIALS

The interim waste storage facility analyzed is located above ground and houses low and intermediate level conditioned waste. The waste is stored within barrels in a crate geometry. The waste repository is modeled using the MCNPX code.

Because the waste in these barrels often is mixed with or enclosed by a layer of concrete to act as a stabilizing and shielding agent, the composition of the waste barrels was modeled as pure concrete (Gualdrini and Ferrari 2003). The waste activity is homogeneously distributed within the barrels. The barrels are stored bottom-to-bottom in a horizontal arrangement within in a crate geometry. The 21 stacking rows each contain 17 pallets of four waste barrels; the pallets are stacked seven high, for a total of 9,996 waste barrels. The rows are separated by 0.85 m to allow a person to walk between stacking rows. The distance between the drum set and the west, north, and east walls is 1 m, with a larger distance of 5.25 m between the drum set and south wall to allow for maneuverability of a crane. The walls are 8.31 m high and composed of concrete; their thickness is 0.2 m with additional shielding of 0.7 m on the west, north, and east walls. A bird's eye view of the facility layout produced using Visual Editor (VISED) (Schwarz et al. 2008) is provided in Fig. 1.

Dose rates around the facility structure were calculated using MCNPX. A conservative estimate for the calculated dose rates outside the facility is provided by modeling the source by ^{60}Co with its relatively long half life (5.27 y) and the two high-energy photons emitted per disintegration (1.173 and 1.332 MeV) (KAERI n.d.). As the individual radionuclide content in each waste barrel is not readily available to personnel outside the operator, and is difficult to model in MCNPX, this approach to providing an upper bound to the dose rates outside the facility was chosen instead. In the model, the source was distributed homogeneously over the volume of the 9,996 waste barrels.

Dose rates were determined using the F5 detector tally (MCNP Team 2008) and ICRP 74 fluence-to-air kerma rate conversion factors (ICRP 1996). Air kerma provides a reasonable approximation for the effective dose to a person for irradiation in the anterior-posterior direction and at photon energies around the ^{60}Co emission energy, and it often closely mirrors detector

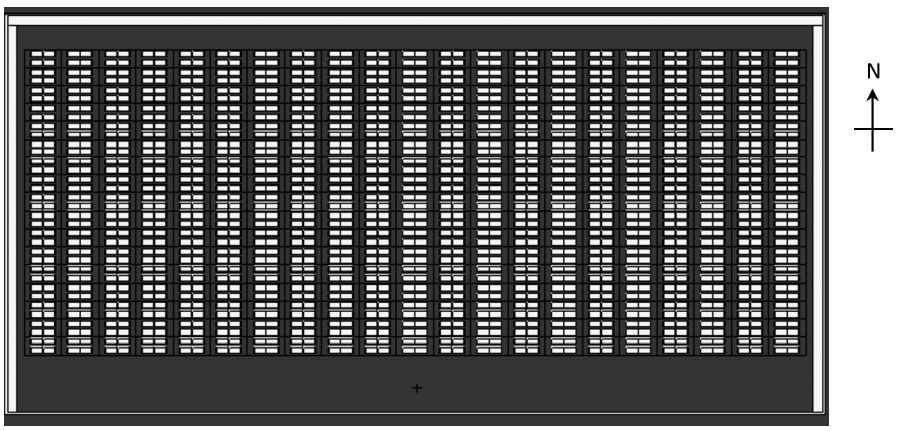

FIG. 1. Bird's eye view of the repository facility.

Copyright © 2018 Health Physics Society. Unauthorized reproduction of this article is prohibited.

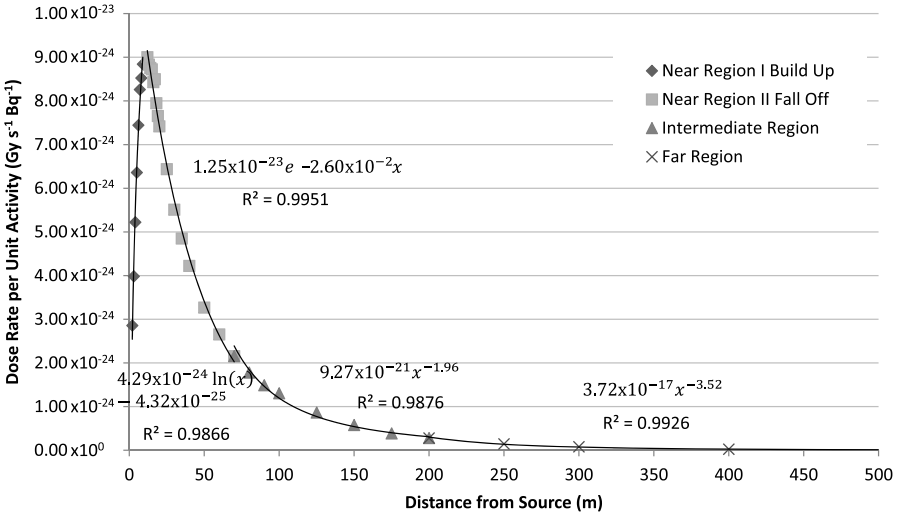

FIG. 2. Typical north side profile with regions labeled.

response. Only for photon energies significantly lower, air kerma deviates from effective dose in that irradiation geometry. Air kerma conversion factors are used to represent the dose rate at the location of the F5 detector tally.

The MCNPX F5 detector tally provides a deterministic estimator of the photon fluence at a point which does not require a particle to reach the detector to contribute to the tally. It was chosen for this analysis to optimize the simulation run lengths, as the particle random walk for other MCNPX tallies becomes inefficient for the large distances from the source simulated in this application. The F5 tally may exhibit unexpected behavior near scattering surfaces or periodic boundary conditions, such as slow or incorrect convergence. The statistical tests on the tally results did not indicate any problematic behavior.

Detector tallies were used to develop horizontal dose rate profiles between 0 and up to 750 m from the waste storage facility for the north, west, and south sides at five heights from the ground: 1.09 m, 2.42 m, 3.75 m, 5.08 m, and 6.41 m. The east side was not analyzed due to symmetry between the east and west sides of the repository. The vertical heights chosen span from the ground to the roof of the repository. The dose rate profiles were divided into several regions based on graphical features and fit of analytical functions.

RESULTS AND DISCUSSION

Dose rates per unit activity were plotted against distance from the facility drum set for the north, west, and south sides of the facility for five tally heights. Observed phenomena in the dose rate profiles depended on the side of the facility studied. Trends for the north and west sides of the facility, where additional shielding with a thickness 0.7 m is applied, are similar at all tally heights. The dose rate initially increases to a maximum within 30 m of the waste storage facility and subsequently decreases rapidly. For the south side of the facility, where no additional shielding is present, the dose rate decreases continuously. These trends are observed in the fluence rate profiles as well, indicating that they are actually due to increased gamma fluences rather than being the result of the ICRP 74 fluence-to-dose rate conversion factors.

For the north and west sides of the facility, four distinct regions were identified: near region I, near region II, intermediate region, and far region (Fig. 2). The near region I, where dose rates increase to a maximum, is best characterized using a logarithmic function, consistent with previously modeled extended sources (Zoeger and Brandl 2011). Beyond the maximum, dose rates are best characterized using an exponential function within the near region II; the expected power law function did not provide a suitable fit in that region. Following the near regions, dose rates are characterized using power functions.

For the south side of the facility, three distinct regions were identified (Fig. 3): a near region, an intermediate region, and a far region. All three regions are characterized by power functions. The near region corresponds closely to the dose rate profile from an infinite plane source (exponent close to −1), the far region corresponds

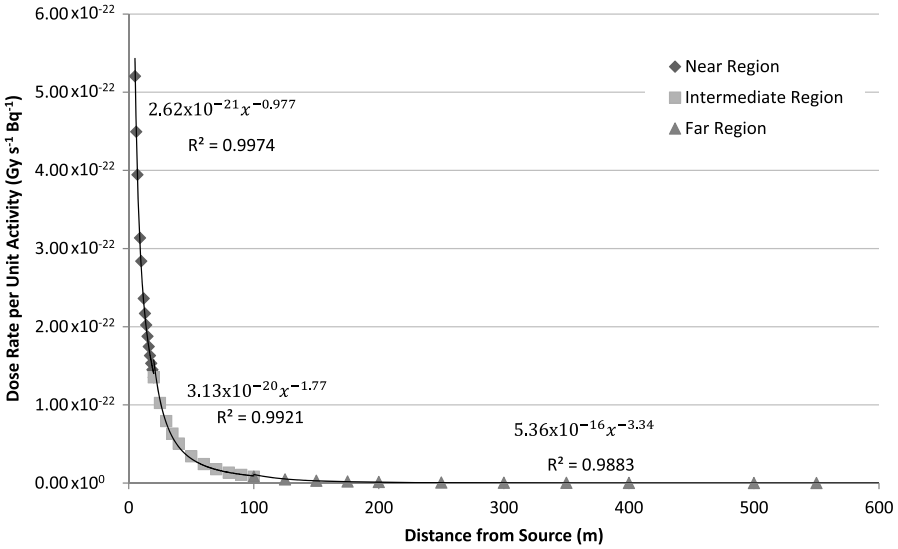

FIG. 3. Typical south side profile with regions labeled.

Copyright © 2018 Health Physics Society. Unauthorized reproduction of this article is prohibited.

closely to a point source (exponent close to −2), while the intermediate region follows an exponential dependence between a point source and an infinite plane source.

Region fit data are provided for the north, west, and south sides of the facility in Tables 1, 2, and 3, respectively. Some trends in the fit data are observed. For the near region I of the north and west side, the fit coefficient multiplying the logarithmic function increases with vertical height, indicating that the dose rate rises more rapidly with height, and the peak is reached closer to the facility. The presence of the peak dose rate closer to the facility is also apparent in Table 4, which lists the peak dose rate locations with vertical height for the north and west sides of the facility.

Additionally, the power of the exponential fit for near region II for the north and west sides decreases with vertical height (becomes more negative); indicating that, beyond the peak, dose rates decrease more rapidly with vertical height. The fit coefficient for the exponential function increases with vertical height, due to the increased peak dose rate with vertical height. The near region on the south side is characterized by a power function closely mirroring the functional dependence of an infinite plane source (exponent approximately −1).

In the intermediate region for all repository sides, the value of the exponent in the power function is between −1 and −2.05, indicating that the dose rate falls off approximately between the functional behavior expected for a planar and point source. In the far region, the value of the exponent in the power function is less than −2 (more negative), indicating that the dose rate falls off more rapidly than expected from the point source approximation. It should also be noted that the fit coefficient for the far region is several orders of magnitude larger than the dose rate at the wall. For the near (south side), intermediate, and far regions, the

Table 1. Region fit data for the north side.

		North – vertical height				
		1.09 m	2.42 m	3.75 m	5.08 m	6.41 m
Near Region I	Eq. (Gy s^{-1} Bq^{-1})	$1.87\times10^{-24}\ln(x)+7.38\times10^{-25}$	$2.33\times10^{-24}\ln(x)-6.02\times10^{-25}$	$3.10\times10^{-24}\ln(x)+3.8\times10^{-25}$	$3.19\times10^{-24}\ln(x)+2.27\times10^{-25}$	$4.69\times10^{-24}\ln(x)-9.12\times10^{-25}$
	R^2	0.979	0.992	0.957	0.966	0.970
	Bounds (m)	3 – 16	4 – 16	3 – 12	3 – 10	3 – 9
Near Region II	Eq. (Gy s^{-1} Bq^{-1})	$8.25\times10^{-24}e^{-1.84\times10^{-2}x}$	$9.26\times10^{-24}e^{-1.94\times10^{-2}x}$	$1.01\times10^{-23}e^{-2.03\times10^{-2}x}$	$1.03\times10^{-23}e^{-1.97\times10^{-2}x}$	$1.16\times10^{-23}e^{-2.05\times10^{-2}x}$
	R^2	0.998	0.994	0.996	0.999	0.999
	Bounds (m)	20 – 70	25 – 80	17 – 80	16 – 80	13 – 70
Intermediate Region	Eq. (Gy s^{-1} Bq^{-1})	$6.97\times10^{-21}x^{-1.87}$	$1.04\times10^{-20}x^{-1.94}$	$9.15\times10^{-21}x^{-1.90}$	$1.55\times10^{-20}x^{-2.02}$	$8.97\times10^{-21}x^{-1.89}$
	R^2	0.993	0.995	0.993	0.996	0.993
	Bounds (m)	70 – 175	80 – 175	80 – 175	80 – 200	70 – 175
Far Region	Eq. (Gy s^{-1} Bq^{-1})	$2.49\times10^{-17}x^{-3.45}$	$9.42\times10^{-18}x^{-3.25}$	$1.44\times10^{-17}x^{-3.33}$	$8.41\times10^{-17}x^{-3.64}$	$1.26\times10^{-16}x^{-3.73}$
	R^2	0.998	0.992	0.991	0.997	0.988
	Bounds (m)	175 – 400	175 – 350	175 – 350	200 – 400	175 – 550

Table 2. Region fit data for the west side.

		West – vertical height				
		1.09 m	2.42 m	3.75 m	5.08 m	6.41 m
Near Region I	Eq. (Gy s^{-1} Bq^{-1})	$2.69\times10^{-24}\ln(x)-1.21\times10^{-25}$	$3.11\times10^{-24}\ln(x)+8.52\times10^{-26}$	$4.29\times10^{-24}\ln(x)-4.32\times10^{-25}$	$6.05\times10^{-24}\ln(x)-9.52\times10^{-25}$	$9.50\times10^{-24}\ln(x)-1.58\times10^{-24}$
	R^2	0.985	0.985	0.987	0.991	0.980
	Bounds (m)	3 – 14	2 – 11	2 – 9	2 – 8	2 – 7
Near Region II	Eq. (Gy s^{-1} Bq^{-1})	$9.27\times10^{-24}e^{-2.13\times10^{-2}x}$	$1.07\times10^{-23}e^{-2.36\times10^{-2}x}$	$1.25\times10^{-23}e^{-2.60\times10^{-2}x}$	$1.47\times10^{-23}e^{-2.84\times10^{-2}x}$	$2.12\times10^{-23}e^{-3.97\times10^{-2}x}$
	R^2	0.998	0.999	0.995	0.993	0.991
	Bounds (m)	15 – 80	15 – 70	12 – 70	10 – 70	7 – 40
Intermediate Region	Eq. (Gy s^{-1} Bq^{-1})	$5.00\times10^{-21}x^{-1.81}$	$7.20\times10^{-21}x^{-1.90}$	$9.27\times10^{-21}x^{-1.96}$	$6.64\times10^{-21}x^{-1.86}$	$1.46\times10^{-21}x^{-1.53}$
	R^2	0.997	0.992	0.988	0.993	0.987
	Bounds (m)	80 – 150	70 – 200	70 – 200	70 – 175	40 – 150
Far Region	Eq. (Gy s^{-1} Bq^{-1})	$4.96\times10^{-19}x^{-2.73}$	$4.24\times10^{-16}x^{-3.96}$	$3.72\times10^{-17}x^{-3.52}$	$1.61\times10^{-17}x^{-3.37}$	$3.47\times10^{-19}x^{-2.64}$
	R^2	0.996	0.989	0.993	0.989	0.998
	Bounds (m)	150 – 300	200 – 500	200 – 400	175 – 400	150 – 250

Copyright © 2018 Health Physics Society. Unauthorized reproduction of this article is prohibited.

Table 3. Region fit data for the south side.

		South – vertical height				
		1.09 m	2.42 m	3.75 m	5.08 m	6.41 m
Near Region	Eq. (Gy s^{-1} Bq^{-1})	$1.25\times10^{-21}x^{-7.33\times10^{-1}}$	$2.58\times10^{-21}x^{-9.92\times10^{-1}}$	$2.62\times10^{-21}x^{-9.77\times10^{-1}}$	$2.53\times10^{-21}x^{-9.67\times10^{-1}}$	$1.90\times10^{-21}x^{-8.67\times10^{-1}}$
	R^2	0.985	0.992	0.997	0.992	0.982
	Bounds (m)	5 – 20	5 – 25	5 – 20	5 – 25	5 – 25
Intermediate Region	Eq. (Gy s^{-1} Bq^{-1})	$4.34\times10^{-20}x^{-1.87}$	$9.09\times10^{-20}x^{-2.03}$	$3.13\times10^{-20}x^{-1.77}$	$6.89\times10^{-20}x^{-1.97}$	$8.81\times10^{-20}x^{-2.03}$
	R^2	0.985	0.993	0.992	0.990	0.988
	Bounds (m)	20 – 150	25 – 150	20 – 100	25 – 150	25 – 175
Far Region	Eq. (Gy s^{-1} Bq^{-1})	$4.13\times10^{-15}x^{-4.13}$	$1.35\times10^{-15}x^{-3.92}$	$5.36\times10^{-16}x^{-3.34}$	$1.13\times10^{-15}x^{-3.88}$	$8.76\times10^{-16}x^{-3.92}$
	R^2	0.986	0.987	0.988	0.9926	0.989
	Bounds (m)	150 – 750	150 – 700	100 – 550	150 – 650	175 – 700

Table 4. Peak location for different vertical heights.

	Vertical height (m)	Peak location (m)
North	1.09	20
	2.42	18
	3.75	12
	5.08	11
	6.41	10
West	1.09	13
	2.42	12
	3.75	10
	5.08	9.0
	6.41	7.0

fit coefficient for the power function increases with distance from the repository. If the dose rate was truly behaving like a point source or line source, the fit coefficient should be constant and similar to the dose rate at the wall. The increase in the fit coefficient and steeper decrease than expected (exponent in the power function less than −2) indicate that other contributions, such as from scattering, do not reach further distances.

The presence of a peak in the dose rate profile is of concern in the analysis of the maximum dose rate outside the facility for safety reasons. Table 5 provides a comparison of the dose rate incident on the wall, 1 m away from the repository and the peak dose rate. For the north and south sides of the facility, the peak dose rate is larger than the dose rate incident on the wall by up to a factor of three. Additionally, the dose rate incident on the wall is lower than the dose rate 1 m away from the facility wall for the north and west sides. The most conservative dose estimates for the north and west sides are obtained at the peak location. The most conservative dose estimate for the south side results from radiation incident on the wall.

CONCLUSION

The dose rate surrounding a waste storage facility was analyzed for a facility handling low and intermediate level conditioned waste. The facility is shielded by a wall of .09 m thickness on the north, west, and east sides; the south side exhibits a 5.25-m air gap and a subsequent wall of thickness 0.2 m. The dose rate profile was analyzed using MCNPX for heights of 1.09 m, 2.42 m, 3.75 m, 5.08 m, and 6.41 m for the north, west, and south sides of the repository. A peak in the dose rate is observed for the north and west sides of the facility. The dose rate profile is expected to decrease following a power function similar to an infinite plane source (exponent of −1). The peak present in the dose rate profiles indicates additional contributions to the dose rate profile from scattering in the shielding material or air similar to the effects observed from skyshine.

In the far regions for the north, west, and south sides, the power function fit for the dose rate profile exhibits an exponent less than −2

Table 5. Dose rate at wall, 1 m from repository, and peak dose rate.

		Dose rate/unit activity (Gy s^{-1} Bq^{-1})				
		Incident on wall	1 m from facility	Peak	Incident on wall/1 m from facility	Peak/1 m from facility
North	1.09 m	2.29×10^{-24}	2.99×10^{-24}	5.68×10^{-24}	77%	190%
	2.42 m	2.36×10^{-24}	3.38×10^{-24}	5.82×10^{-24}	70%	172%
	3.75 m	2.56×10^{-24}	3.82×10^{-24}	7.57×10^{-24}	67%	198%
	5.08 m	2.77×10^{-24}	4.29×10^{-24}	7.49×10^{-24}	65%	175%
	6.41 m	3.46×10^{-24}	5.45×10^{-24}	8.95×10^{-24}	64%	164%
West	1.09 m	1.56×10^{-24}	2.48×10^{-24}	6.69×10^{-24}	63%	269%
	2.42 m	1.75×10^{-24}	2.91×10^{-24}	7.53×10^{-24}	60%	258%
	3.75 m	1.92×10^{-24}	3.45×10^{-24}	8.83×10^{-24}	56%	256%
	5.08 m	2.14×10^{-24}	4.43×10^{-24}	1.14×10^{-23}	48%	257%
	6.41 m	2.34×10^{-24}	6.35×10^{-24}	1.59×10^{-23}	37%	251%
South	1.09 m	3.70×10^{-22}	3.38×10^{-22}	—	109%	—
	2.42 m	8.22×10^{-22}	4.58×10^{-22}	—	179%	—
	3.75 m	6.73×10^{-22}	4.87×10^{-22}	—	138%	—
	5.08 m	5.25×10^{-22}	4.76×10^{-22}	—	110%	—
	6.41 m	4.77×10^{-22}	4.02×10^{-22}	—	119%	—

Copyright © 2018 Health Physics Society. Unauthorized reproduction of this article is prohibited.

(more negative). This means that the dose rate falls off more rapidly than for a point source, indicating that additional contributions, such as scattering, occur for distances closer to the repository. To provide a maximum dose analysis, doses should be evaluated at the peak locations for the north and west sides of facility; for the south side, dose rates are a maximum at the wall of the facility.

Acknowledgments—We thank Nuclear Engineering Seibersdorf for providing an interesting research question and facility drawings. We thank Rafe McBeth for running the MCNP files on the CSU computer cluster and assisting in debugging the code. In addition, we thank Thomas McLean and David Seagraves at Los Alamos National Laboratory for their assistance in developing the repeated source structure.

This publication was supported by Grant Number T42OH009229-06 from the CDC NIOSH Mountain and Plains Education and Research Center. Its contents are solely the responsibility of the authors and do not necessarily represent the official views of the CDC NIOSH and MAP ERC.

REFERENCES

Bevelacqua JJ. Point source approximations in health physics. Radiat Protect Manag 21:9–13; 2004.

Bonnet C, Hillion P, Nurdin G. Calcul de l'angle solide source detecteur. Nucl Instrum Methods Phys Res Sect A 54:321–322; 1967 (in French).

Carchon R, Van Camp E, Knuyt G, Van De Vyver R, Devos J, Ferdinande H. A general solid angle calculation by Monte Carlo method. Nucl Instrum Meth 128:195–199; 1975. DOI: 10.1016/0029-554X(75)90796-X.

Forty CBA. Gamma radiation fields around the cooling circuits of a fusion power plant. Wetherby: UKAEA; UKAEA; 1996.

Gardner RP, Carnesale A. The solid angle subtended at a point by a circular disk. Nucl Instrum Meth Phys Res Sect A 73:288–230; 1969.

Gotoh H, Yagi H. Solid angle subtended by a rectangular slit. Nucl Instrum Meth Phys Res Sect A 96:485–486; 1971.

Green M, Aadmodt R, Johnston G. The solid angle subtended by a solid, right, circular cylinder as seen from a point in space. Nucl Instrum Meth Phys Res Sect A 117:409–412; 1974 DOI: 10.1016/0029-554X(74)90285-7.

Gualdrini G, Ferrari P. Proceedings of the International Workshop on Intercomparison on the Usage of Computational Codes in Radiation Dosimetry. ENEA: Bologna; 2003.

International Commission on Radiological Protection. Conversion coefficients of use in radiological protection against external radiation. Oxford: Pergamon Press; ICRP Publication 74, Ann ICRP 26(3/4); 1996.

Jaffey AH. Solid angle subtended by a circular aperture at point and spread sources: formulas and some tables. Rev Sci Instrum 24: 349–354; 1954 DOI: 10.1063/1.1771061.

Johnson TE, Birky BK. Health physics and radiological health. Baltimore: Lippincott Williams & Wilkins; 2012.

Korean Atomic Energy Research Institute. 27-cobalt-60 [online]. Available at ***http://atom.kaeri.re.kr/ton/nuc9.html***. Accessed 1 October 2013.

Kontogeorgakos D, Tzika F, Valakis S, Stamatelatos IE. Occupational radiation exposure during removal of radioactive reactor components from GRR-1 pool. Radiat Protect Dosim 144:632–635; 2011 DOI: 10.1093/rpd/ncq335.

Koukorava C, Carinou E, Ferrari P, Krim S, Struelens L. Study of the parameters affecting operator doses in interventional radiology using Monte Carlo simulations. Radiat Meas 46:1216–1222; 2011 DOI: 10.1016/j.radmeas.2011.06.057.

Monte Carlo N-Particle eXtended Team. Monte Carlo n-particle extended. Los Alamos: Los Alamos National Laboratory; 2008.

Rizk RA, Hathout AM, Hussein ARZ. On solid angle calculation. Nucl Instrum Meth Phys Res Sect A 245:162–166; 1986 DOI: 10.1016/0168-9002(86)90271-8.

Rogers DWO. Fifty years of Monte Carlo simulations for medical physics. Phys Med Biol 51: 287–301; 2006.

Schwarz AL, Schwarz RA, Carter LL. MCNP/MCNPX Visual Editor Computer Code. Richland: Schwarz Software & Consulting, LLC; 2008.

Siiskonen T, Tapiovaara M, Kosunen A, Lehtinen M, Vartiainen E. Monte Carlo simulations of occupational radiation doses in interventional radiology. Br J Radiol 80:460–468; 2014.

Verghese K, Gardner RP, Felder RM. Solid angle subtended by a circular cylinder. Nucl Instrum Meth Phys Res Sect A 101:391–393; 1972 DOI: 10.1016/0029-554X(72)90214-5.

Wielopolaki L. The Monte Carlo calculation of the average solid angle subtended by a right circular cylinder from distributed sources. Nucl Instrum Meth Phys Res Sect A 143:577–581; 1977 DOI: 10.1016/0029-554X(77)90249-X.

Williams IR. Monte Carlo calculation of source-to-detector geometry. Nucl Instrum Meth Phys Res Sect A 44:160–162; 1966 DOI: 10.1016/0029-554X(68)90082-7.

Zoeger N, Brandl A. Dose rate distribution from a standard waste drum arrangement. Health Phys 101:142–147; 2011 DOI: 10.1097/HP.0b013e3182295943.

Copyright © 2018 Health Physics Society. Unauthorized reproduction of this article is prohibited.